Research Article

Kena Sun, Xiaowu Jie*, Yonglu Zhang, Zhichao Yao, Wei Gao, Wenyi He, and Guanjin Gao

Exploring the selective enrichment of vanadium–titanium magnetite concentrate through metallization reduction roasting under the action of additives

https://doi.org/10.1515/htmp-2025-0073
received January 15, 2025; accepted February 17, 2025

Abstract: To achieve comprehensive recovery and utilization of iron and titanium resources in vanadium titanium magnetite concentrate, the vanadium titanium magnetite concentrate is subjected to metallization reduction roasting, studying the selective enrichment effects on iron- and titanium-containing phases in the reduction products under the influence of additives. Experimental results indicate that elevating reduction temperature, increasing additive concentration, and extending the reduction time promote the aggregation and growth of phases containing iron and titanium in the reduction products. Under the optimized roasting conditions of 1,250°C, addition of 4% of the additive, and a reduction time of 3 h, 92.91% of iron existed in metallic form, and 87.35% of titanium existed as anosovite. The average equivalent circle diameters for iron and titanium particles are 45.3 and 10.1 μm, respectively. By magnetic separation of the reduced products, the obtained magnetic separation concentrate contains 93.06% Fe, with an iron recovery rate of 96.15%. The magnetic separation tailings contain 39.22% TiO_2, and the Ti enrichment rate of the tailings is 87.75%, indicating a good separation effect of iron and titanium.

*** Corresponding author: Xiaowu Jie**, BGRIMM Technology Group, Metallurgical Research and Design Institute, Beijing 100081, China; State Key Laboratory of Vanadium and Titanium Resources Comprehensive Utilization, Panzhihua 617000, China, e-mail: jiexiaowu002@163.com
Kena Sun, Wei Gao: BGRIMM Technology Group, Metallurgical Research and Design Institute, Beijing 100081, China
Yonglu Zhang, Zhichao Yao: BGRIMM Technology Group, Metallurgical Research and Design Institute, Beijing 100081, China; State Key Laboratory of Vanadium and Titanium Resources Comprehensive Utilization, Panzhihua 617000, China
Wenyi He, Guanjin Gao: State Key Laboratory of Vanadium and Titanium Resources Comprehensive Utilization, Panzhihua 617000, China

Keywords: vanadium–titanium magnetite concentrate, metallization reduction, iron, anosovite, particle growth

1 Introduction

Vanadium–titanium magnetite is a typical polymetallic-associated mineral resource containing iron, vanadium, and titanium as its main elements [1,2]. China has proven long-term reserves of over 30 billion tons [3,4], of which the remaining reserves in the Panxi region are over 10 billion tons [5]; its titanium and vanadium reserves account for 35.2 and 11.6% of the world's total reserves, respectively [6]. Due to its abundant iron, vanadium, and titanium resources, it holds significant value for comprehensive utilization. Vanadium–titanium magnetite concentrate, obtained through ore dressing, is a crucial raw material for iron smelting and vanadium extraction [7,8], of which iron accounts for 60–80% of the total iron in the raw ore, titanium accounts for 85–90% of the total vanadium in the raw ore [9]. According to the differences in ore properties, there are currently three main industrial methods for processing vanadium titanium magnetite concentrate. China and Russia mainly use the blast furnace converter process, which can effectively recover iron and vanadium [10,11]. However, titanium will enter the blast furnace slag (the TiO_2 grade in the blast furnace slag is as high as 22–25%) [12,13]. Due to technical and economic limitations, this part of TiO_2 cannot be efficiently recovered, resulting in a huge waste of titanium resources [14,15]. South Africa and New Zealand adopted the rotary kiln direct reduction electric furnace smelting process; however , this process just recovers the elements of Fe and V [16–18].

To achieve effective separation of iron and titanium in titanium magnetite concentrate, researchers have extensively studied the thermodynamics and reaction processes of the reduction of vanadium–titanium magnetite concentrate both domestically and internationally and developed

non-blast furnace smelting methods such as direct reduction [19,20] and reduction melting [21]. Roshchin et al. [22] used a two-step processing to treat titaniferous magnetite ore concentrates, and the processing includes solid-phase reduction of iron and separation melting of the reduction products, which provides a complete recovery of iron into a metallic phase at the maximum titanium oxide content in a slag. Chen et al. [23], Chen and Chu [24], and Wei et al. [25] analyzed the X-ray diffraction (XRD) patterns of reduction products at different times and concluded that magnetite and ilmenite in the concentrate react sequentially through staged reduction. The reduction paths for magnetite and ilmenite are $Fe_3O_4 \rightarrow FeO \rightarrow Fe$ and $Fe_2TiO_5 \rightarrow Fe_2TiO_4 \rightarrow FeTiO_3 \rightarrow FeTi_2O_5 \rightarrow TiO_2$, respectively. Hu et al. [26,27] conducted thermodynamic calculations and physical analysis to study the reaction process of coal-based direct reduction of vanadium–titanium magnetite concentrates under isothermal and non-isothermal conditions. Zulhan et al. [28,29] found that temperature patterns and briquette thickness directly affect the formation of iron nuggets in the fluxless processing of titanomagnetite. Their study provides insights into the challenges associated with direct reduction. To alleviate these difficulties, the reduction process is enhanced primarily using additives. Chen et al. [30,31] studied the effect of Na_2CO_3 and CaF_2 as additives on the reduction performance of the concentrate. Zhang et al. [32] and Gao et al. [33] found that employing CaF_2 and NaF as additives can effectively reduce the activation energy of carbon-containing pellets. Jiang's et al. [34] and Yang et al. [35] on high-chromium vanadium–titanium magnetite with coal-based direct reduction also indicated that under the condition of carbon ratio of 1.2, temperature of 1,250°C, and reaction time of 30 min, the maximum metallization rate is 85.27% with 3% CaF_2 addition. Chen et al. [36,37] investigated the influence of different magnesium compounds on the reduction of vanadium–titanium magnetite in coke powder reduction. Gas analysis results showed that, following reduction at 1,250°C for 120 min, the reduction degree of pellets with different magnesium compounds followed the order: $MgCl_2$ > MgO > $Mg(OH)_2$ > no additive > $MgSO_4$. Li et al. [38,39] found that for single additives, potassium salt roasting additives are more efficient than sodium and calcium salts, and K_2SO_4 has the best effect among them. Moreover, composite roasting additives such as K_2SO_4/KCl perform better than single potassium salt additives, and the vanadium leaching efficiency can reach 82.04%.

Existing research indicates that using carbon-based reducing agents facilitates the gradual dissociation of titanium magnetite and the reduction of elemental iron. However, during the reduction process, the generated iron particles typically possess a size below 20 μm, rendering individual dissociation difficult during the grinding process and hindering subsequent magnetic enrichment [40]. This study focuses on vanadium–titanium magnetite concentrate as the raw material, using a self-prepared composite additive as an additive; the study particularly investigates the impact of reduction temperature, additive quantity, and roasting time, as well as their influence on the distribution of newly formed iron and anosovite phases and their particle size. This research aims to provide a theoretical basis for the metallization roasting and magnetic separation of vanadium–titanium magnetite concentrate.

2 Experimental

2.1 Materials

The experimental materials mainly include vanadium titanium magnetite concentrate from the Panzhihua area of Sichuan, reducing agent, and additive. The chemical composition analysis results of the vanadium–titanium magnetite concentrate are presented in Table 1. The ore exhibits high iron content and a substantial TiO_2 content, indicating its potential for recycling. The XRD pattern analysis is shown in Figure 1, revealing four main phases in the vanadium–titanium magnetite: magnetite, ilmenite, magnesium olivine, and a complex silicate of calcium, magnesium, iron, and aluminum.

Table 1: Main compositions of vanadium–titanium magnetite concentrates (mass fraction)

Component	Fe	TiO_2	V	SiO_2	CaO	MgO	Al_2O_3
Content (%)	52.62	13.44	0.28	2.68	0.75	3.23	3.80

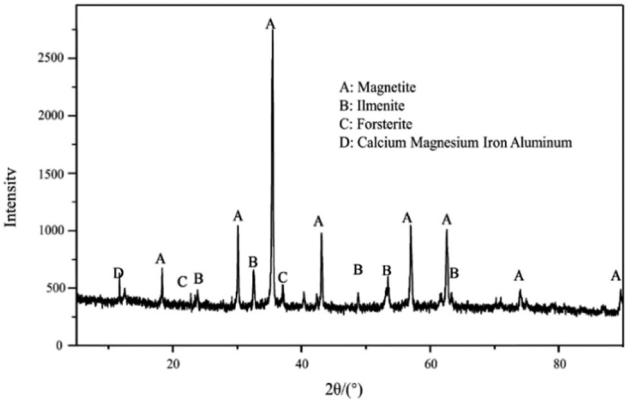

Figure 1: XRD patterns of vanadium–titanium magnetite concentrates.

Table 2: Industrial analysis of reducing coal (mass fraction)

Component	Fixed carbon	Volatile	Ash content	Total sulfur
Content (%)	58.77	31.97	9.26	0.32

A low-sulfur bituminous coal (particle size 3 mm) was used as the reducing agent. Its main physical characteristics are summarized in Table 2. The composite additive used in the experiment is mainly composed of $CaCl_2$ and NaCl, with a mass ratio of 3:7. Grind $CaCl_2$ and NaCl separately to a fine particle size according to the above-mentioned ratio and then transfer them to a V-type mixer. Set the rotation speed at 15 rpm and the mixing time at 10 min to ensure sufficient contact between the agents.

2.2 Experimental procedure

Finely ground vanadium–titanium magnetite concentrate, 30% of the reducing agent, and varying amounts of the additive (from 0 to 6%) were mixed according to the designed ratio (by mass). After natural drying, 5% of water and 0.1–0.5% of a binder (polyacrylamide solution) were added and mixed to form granules. The granules, with a diameter of 10–20 mm, were dried in a drying oven at 100°C for 2 h, resulting in pellets as shown in Figure 2(a). These dried pellets were loaded into alumina crucibles, sealed, and placed in a high-temperature resistance furnace. The temperature was raised from room temperature at a controlled rate of 6–8°C·min^{-1}. After reaching the preset temperature, isothermal roasting was conducted, and the reduction was completed with water-sealed slow cooling. The obtained reduction products are illustrated in Figure 2(b), with an average size of approximately 8–18 mm, which is slightly smaller than that of the dried pellets before roasting.

2.3 Analysis methods

Scanning electron microscopy (SEM) and energy-dispersive X-ray spectroscopy (EDS) were used to characterize the morphology and the phase composition of the reduction products. The particle size of metallic iron and anosovite was determined using a BGRIMM Process Mineralogy Analyzing System. The particle size characteristics of metallic iron were described using parameters such as minimum span and equivalent circle diameter. The minimum span represents the particle size that can pass through a sieve, while the equivalent circle diameter represents the diameter of a circle having an area equivalent to that of the particle after removing internal pores. The particle size of anosovite was characterized using the equivalent circle diameter parameter based on its embedding characteristics and image extraction.

3 Results and discussion

Reasonable roasting conditions are the key to achieving efficient separation of iron and impurity components in the metallization reduction – direct magnetic separation process. Therefore, this section focuses on the effects of reduction temperature, additive concentration, and reduction time on the reduction products.

3.1 Influence of reduction roasting factors

3.1.1 Effect of reduction temperature

The reduction temperature is one of the crucial factors influencing the metallization reduction process. To maximize the

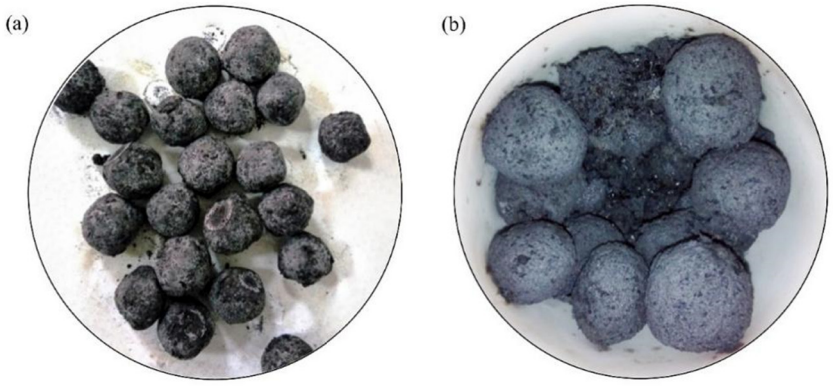

Figure 2: Experimental products: (a) dried pellets and (b) reduction products.

reduction of iron in the vanadium–titanium magnetite concentrate, there must be a sufficient amount of directly reduced iron in the reduction products, leading to the generation of liquid-phase iron and its subsequent crystallization and growth. Referring to the Fe–C binary phase diagram, the appearance of liquid-phase iron begins at 1,148°C [41]. Therefore, based on thermodynamic data, metallization reduction roasting experiments were conducted at different temperatures (1,150, 1,200, 1,250, and 1,300°C) under the conditions of adding 4% additive to the vanadium–titanium magnetite concentrate and maintaining a constant temperature for 3 h. The SEM results of the reduction products at different reduction temperatures are shown in Figure 3.

At 1,150°C, metallic iron appeared in fine-grained and worm-like structures, with an average equivalent circle diameter of 8.2 μm and a minimum span average particle size of 9.8 μm. Anosovite particles were relatively small, with an average equivalent circle diameter of 3.2 μm. At 1,200°C, both metallic iron and anosovite particles slightly increased in size – with average equivalent circle diameters of 10.3 and 5.1 μm, respectively – and the interface between anosovite and silicate became clearer. At 1,250°C, metallic iron exhibited significant growth, transitioning from thin strips to elliptical shapes with internal pores. Anosovite morphology also changed from dot-like to elongated, with average equivalent circle diameters of 30.2 and 10.4 μm. When the temperature rose to 1,300°C, metallic iron particles connected into blocks – with an average equivalent circle diameter of 95 μm – and anosovite particles agglomerated and fused with silicate, resulting in less distinct boundaries.

The experimental results indicate that increasing the temperature promotes the reduction reaction. However, at 1,300°C, the separation of titanium-bearing phases in the reduction products deteriorated. Additionally, iron particles were small and dispersed below 1,250°C. Therefore, 1,250°C was chosen as the optimal reduction temperature.

3.1.2 Effect of additive addition

Different amounts of the additive (0, 2, 4, and 6%) were added during the pelletization process. Roasting

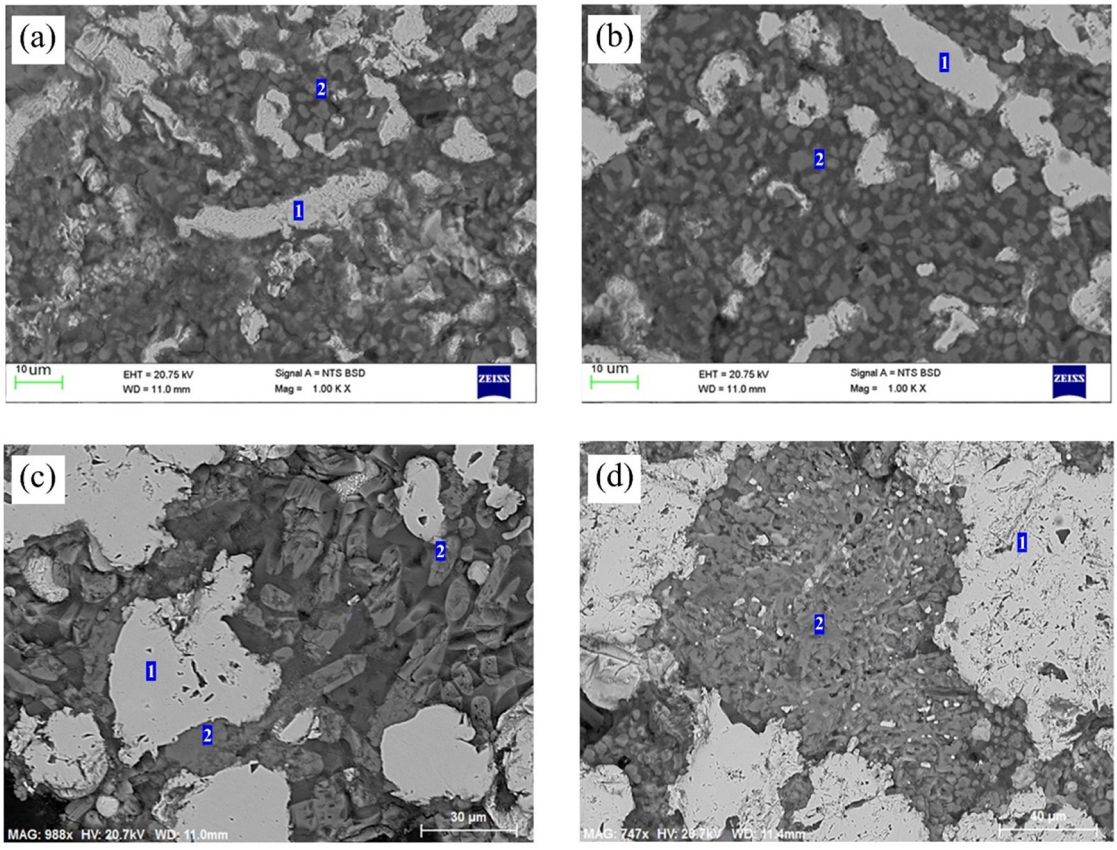

Figure 3: SEM image of the reduced product under different reduction temperatures: (a) 1,150°C; (b) 1,200°C; (c) 1,250°C; and (d) 1,300°C. 1, Metallic iron; 2, anosovite.

experiments were conducted at 1,250°C with a reduction time of 3 h.

Figure 4 depicts the SEM results of the reduction products with varying amounts of the additive, demonstrating that it significantly enhanced the growth of iron and anosovite particles. As the amount of additive increased, growth and aggregation of mineral particles became evident. In the absence of the additive, metallic iron appeared fine-grained and droplet-like, with an average equivalent circle diameter of 15.4 μm and a minimum span average particle size of 16.2 μm. Anosovite showed a granular shape with embedded and relatively small particles exhibiting an average equivalent circle diameter of 4 μm. With an additive concentration of 2%, metallic iron and anosovite particles agglomerated, resulting in average equivalent circle diameters of 20.1 and 7.3 μm, respectively. At 4% of the additive, metallic iron demonstrated more pronounced growth, while anosovite transformed from granular to elongated, with average equivalent circle diameters of 45.3 and 10.1 μm. When the added additive reached 6%, iron particles agglomerated and adhered, reaching an average particle size of 100 μm. Additionally, anosovite particles agglomerated and presented less clear boundaries. The experimental results demonstrate that the self-prepared additive effectively enhances the phase transformation of vanadium–titanium magnetite concentrate, reduces grain boundary resistance, and facilitates the lattice migration of iron particles.

3.1.3 Influence of reduction time

Metallization reduction roasting experiments were conducted at 1,250°C with the addition of 4% of the additive and reduction times of 1, 2, 3, and 4 h.

Figure 5 depicts the SEM results of the reduction products at different reduction times, demonstrating the minimal change in the morphology of metallic iron and anosovite occurred during reduction with reduction times of 1–2 h. Metallic iron exhibited a worm-like structure, while anosovite appeared granular, filling the spaces between metallic iron particles along with silicates and other minerals. The average minimum span particle size of metallic iron and anosovite was 23.1 and 31.9 μm, respectively, whereas the corresponding average equivalent circle diameters were 6.5 and 8 μm. No

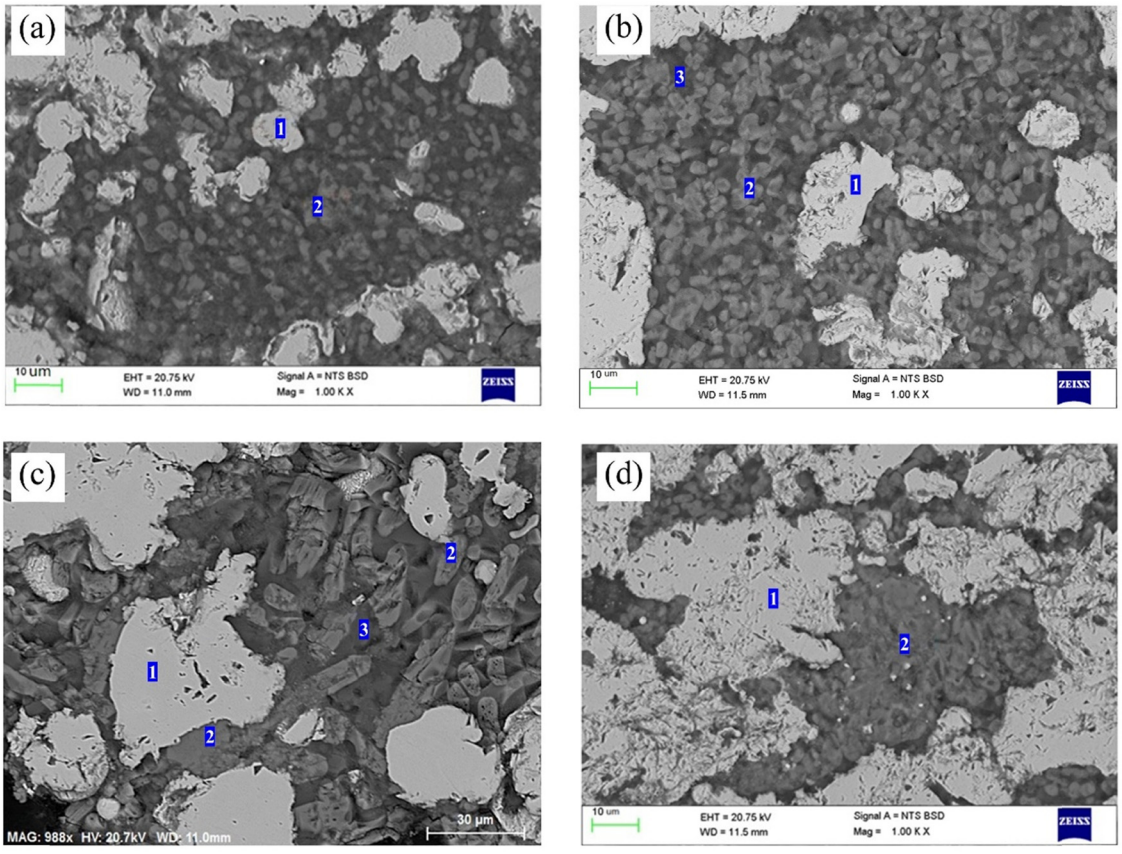

Figure 4: SEM image of the reduced product with different additive addition: (a) 0%; (b) 2%; (c) 4%; and (d) 6%. 1, Metallic iron; 2, anosovite; 3, silicate glass melt.

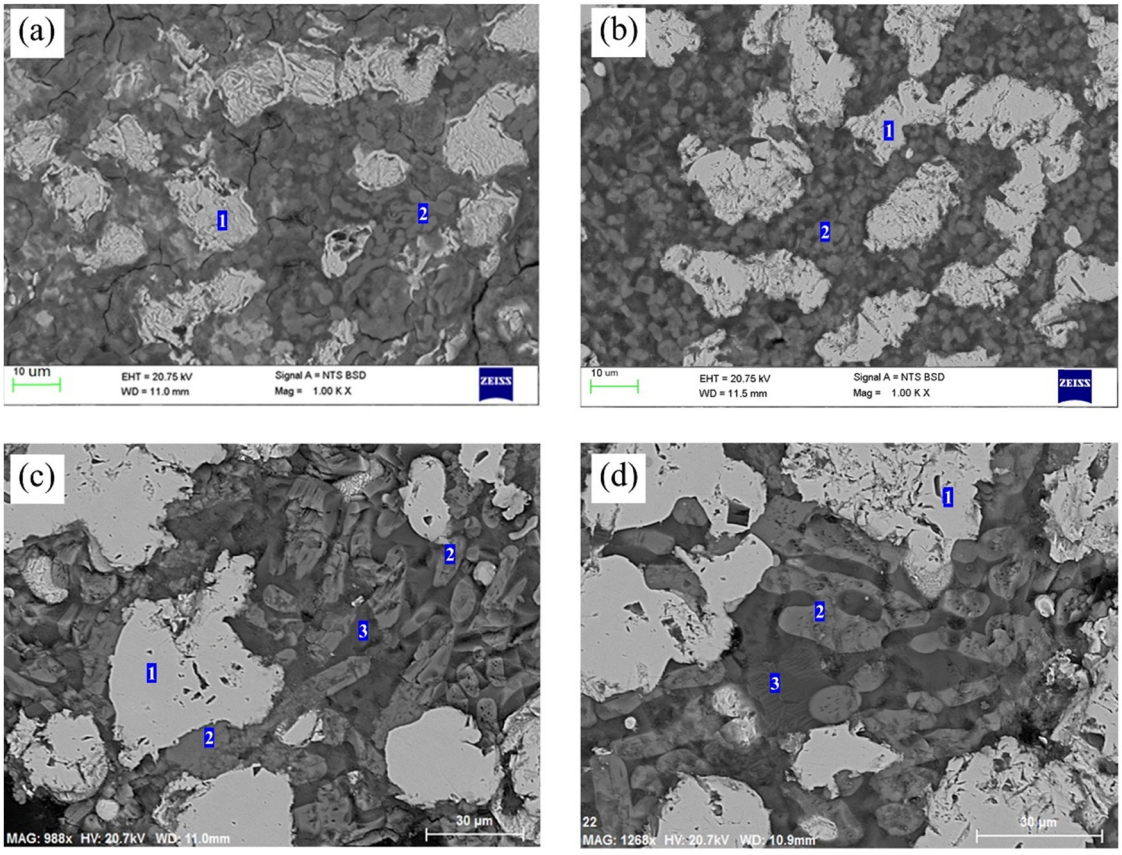

Figure 5: SEM image of the reduced product under different reduction times: (a) 1 h; (b) 2 h; (c) 3 h; and (d) 4 h. 1, Metallic iron; 2, anosovite; and 3, silicate glass melt.

significant increase in particle size was detected when the reduction time was extended to 4 h. These results indicate that, when the reduction time is 3 h or longer, the anosovite in the reduction products can transition from granular to elongated, suggesting that extending the reduction time promotes the aggregation and growth of anosovite.

3.2 Analysis of phases in the reduction products and verification of magnetic separation effects

3.2.1 Main phase composition of the reduction products

Through the analysis of the effects of reduction temperature, additive addition, and reduction time on the Fe and Ti phases in the metalized reduction roasting products, a reduction temperature of 1,250°C, with a 4% additive addition and a reduction time of 3 h, was detected as optimal conditions for the growth of metallic iron and anosovite in the reduction products. With these two phases distinctly separated, the mineral composition of the reduction products under these experimental conditions was examined. The backscattered electron images and EDS analysis of the major phases are shown in Figure 6.

According to Figure 6(b), the total EDS analysis of the reduction products revealed a predominant composition of Fe, Ti, Si, Al, Mg, and O, with minor or trace amounts of elements such as Ca, Na, and S. The chemical analysis of the reduction products is presented in Table 3. Comparing this with the chemical composition of the vanadium–titanium magnetite concentrate before reduction roasting (Table 2), an increase in the content of Fe, TiO_2, and V becomes evident, with a significant increase in the content of Fe by approximately 10%.

Metallic iron was the primary carrier of iron in the reduction products, accounting for about 61% of the total mass. As shown in Figure 6(c), the EDS analysis indicates that metallic iron was mainly composed of Fe, with an average iron content of about 99.68%. The remaining portion consisted of trace amounts of Ti, possibly arising from small titanium-bearing inclusions within metallic iron.

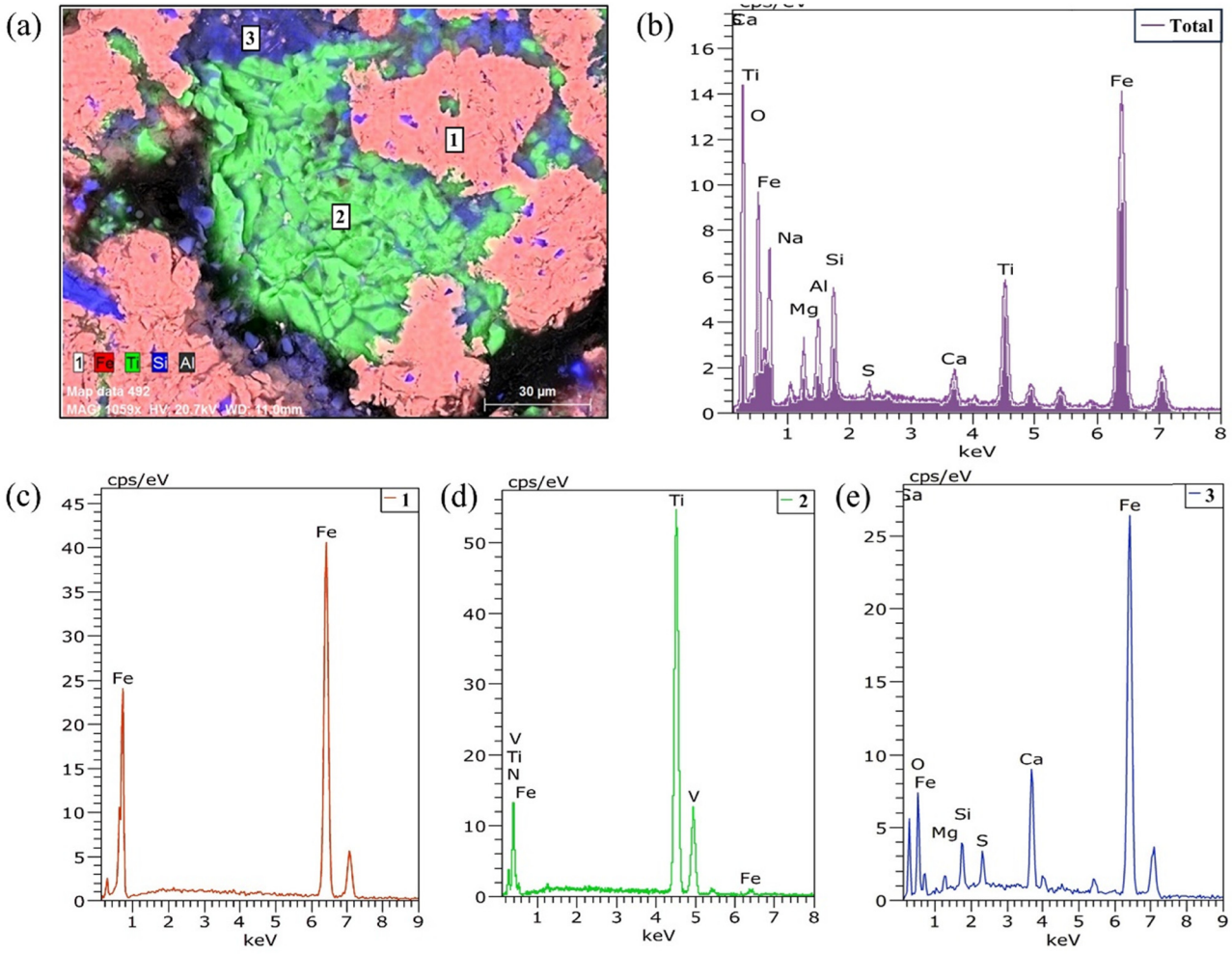

Figure 6: SEM image of reduced products and EDS analysis: (a) SEM image: 1, metallic iron; 2, anosovite; and 3, silicate glass melt; (b) Total EDS spectrum; (c) EDS spectrum of metallic iron at position 1; (d) EDS spectrum of anosovite at position 2; and (e) EDS spectrum of silicate glass melt at position 3.

Anosovite was the major phase carrying titanium in the reduction products, constituting approximately 16% of the total mass. As depicted in Figure 6(d), the EDS analysis reveals that anosovite was primarily composed of Ti and O, with minor amounts of Mg, Al, Fe, and other elements. Anosovite, along with silicate glass melt and other minerals, filled the spaces between metallic iron particles.

Silicate glass melt was the predominant impurity mineral phase in the reduction products, accounting for about 12% of the total mass. As shown in Figure 6(e), the EDS analysis indicates that silicate glass melt mainly consisted of Si, Al, Mg, Na, Ca, and Ti, with additional trace amounts of Cl, Fe, Mn, and other elements. Silicate glass melt existed in a gel-like structure, coexisting with anosovite and magnesium spinel, and was found between metallic iron particles.

Table 3: Chemical composition of reduction products (mass fraction)

Component	TFe	TiO_2	V	SiO_2	CaO	MgO	Al_2O_3
Content (%)	63.08	14.74	0.35	4.87	0.87	3.77	4.42

3.2.2 Composition of other minerals in the reduction products

Other minerals in the reduction products mainly included magnesium spinel and iron oxides, as shown in the SEM and EDS analysis in Figure 7(a) and (b), respectively.

Magnesium spinel constituted approximately 1% of the mineral content. The EDS analysis indicates that magnesium spinel primarily contained Mg, Al, and O, with trace amounts of Ti, Fe, V, and Mn. Magnesium spinel was distributed as fine particles, interspersed with anosovite and silicate glass melt, among metallic iron particles.

Iron oxide in the reduction products constituted approximately 6% of the mineral content. The EDS analysis of iron oxide revealed a predominant composition of Fe and O, with minor amounts of Cl, Ca, Ti, S, and other elements. Iron oxide typically presented a particle size below 100 μm, exhibiting a gel-like structure connected with metallic iron and showing remnants of fine or micro-metal iron structures.

3.2.3 Distribution of iron and titanium in the reduction products

In the reduction products, iron primarily existed in the form of metallic iron, constituting 92.91% of the total iron, whereas 5.62% of iron existed in the form of iron oxide, possibly owing to secondary oxidation during the slow cooling process. Titanium mainly existed in the form of anosovite, which accounted for 87.35% of the total titanium, with an additional 9.65% occurring in association with silicate glass melt. The titanium content in the metallic iron phase was only 2.14%. Iron and titanium in the roasting sands were significantly enriched in their respective capture minerals. Comparison with Figure 1 shows that after the vanadium–titanium magnetite concentrate underwent metalized reduction roasting, most of the iron and titanium in the concentrate transformed from magnetite and ilmenite to metallic iron and anosovite, creating possibilities for subsequent magnetic separation and recovery of valuable metals.

Additionally, Figure 6(a) reveals a significant effect on the migration, aggregation, and growth of iron crystal grains in the reduction products, resulting in sizes reaching into the range of tens or even hundreds of micrometers. Following iron migration, fine anosovite particles aggregated into clusters in the iron-poor region, with particle sizes reaching tens of micrometers. The metallic iron and anosovite phases in the reduction products remained as individual minerals without encapsulation within silicates or other phases. Therefore, under the influence of the additive, the metalized reduction roasting of vanadium–titanium magnetite concentrate achieved selective enrichment of iron and titanium, facilitating the subsequent beneficiation separation and recovery of valuable metals.

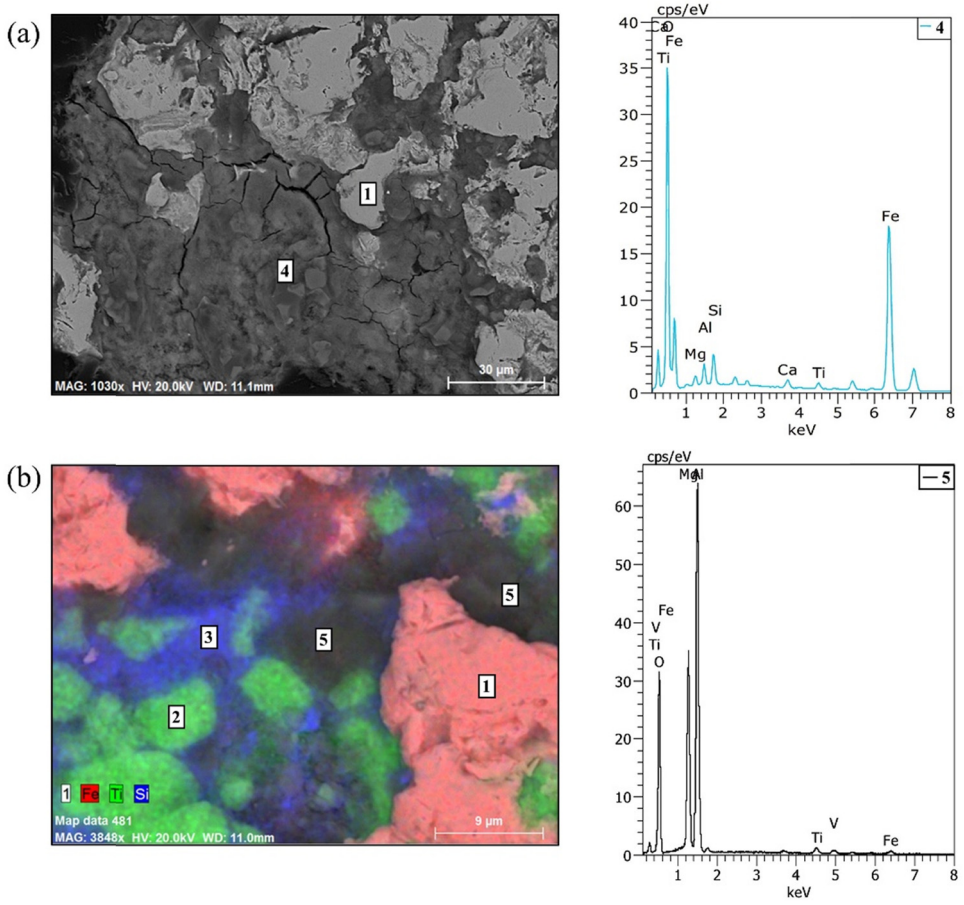

Figure 7: SEM image of reduced products and EDS analysis: 1, metallic iron; 2, anosovite; 3, silicate glass melt; 4, iron oxide; and 5, magnesium spinel. (a) SEM image and the EDS spectrum of the iron oxide at position 4 and (b) SEM image and EDS spectrum of magnesium spinel at position 5.

Table 4: The results of magnetic separation under optimized reduction conditions

Parallel test	Magnetic concentrate (%)			Magnetic separation tailings (%)			Concentrate yield (%)
	Fe	V	TiO_2	Fe	V	TiO_2	
1#	93.05	0.15	2.76	7.81	0.72	38.93	66.41
2#	92.85	0.15	2.92	7.33	0.68	38.64	66.55
3#	93.27	0.14	2.62	6.94	0.76	40.08	66.26
Average	93.06	0.15	2.77	7.36	0.72	39.22	66.40

3.2.4 Magnetic separation effect of iron and titanium in reduction products

The reduction products obtained under optimized roasting conditions are subjected to wet grinding treatment, and the resulting slurry is subjected to magnetic separation at a field strength of 100 mT. The magnetic separation concentrates and tailings are filtered, dried, weighed, and analyzed for Fe, Ti (measured by TiO_2), and V content. To ensure the accuracy of the magnetic separation test results, three sets of parallel magnetic separation tests were conducted, and the results were shown in Table 4.

The experimental results of direct magnetic separation show that the magnetic separation concentrate contains 93.06% Fe, 2.77% TiO_2, and 0.15% V, with a concentrate iron separation rate of 96.15% and a titanium separation rate of 12.25%; The tailings contain 39.22% TiO_2, and the Ti enrichment rate of the tailings is 87.75%, indicating that the reduced products have good magnetic separation effect under this condition.

4 Conclusion

1. Under the optimized roasting conditions of 1,250°C, 4% of the additive, and a reduction time of 3 h, the metallic iron and anosovite phases in the reduction products remained as individual minerals without encapsulation within silicates or other phases. The average equivalent circle diameters for iron and titanium particles are 45.3 and 10.1 μm, respectively.
2. Compared with no additives added, the average equivalent circle diameters for iron and titanium particles in the reduction products increased by 29.9 and 6.1 μm. This indicates that additives can effectively promote the aggregation and growth of iron and titanium phases in the reduced products.
3. The phase analysis indicates that the reduction products under optimized roasting conditions are mainly composed of metallic iron, anosovite, and silicate glass melt, with mineral contents of 61, 16, and 12%, respectively. In addition, they also contain a small amount of magnesium spinel and iron oxide. In the reduction products, 92.91% of the iron primarily existed in metallic form, while 87.35% of the titanium existed as anosovite. The significant enrichment effects within their respective host minerals offer advantages for magnetic separation.
4. After grinding and magnetic separation of the reduction products, the magnetic separation concentrate contains 93.06% Fe, 2.77% TiO_2, and 0.15% V, with a concentrate iron recovery rate of 96.15% and a titanium recovery rate of 12.25%. The tailings contain 39.22% TiO_2, with a Ti enrichment rate of 87.75%, indicating a good separation effect of iron and titanium.

Acknowledgments: The authors gratefully acknowledge financial support from the National Key Research and Development Program of China (2023YFC2908304), and the Open Fund of State Key Laboratory of Vanadium and Titanium Resources Comprehensive Utilization (2021P4FZG02A).

Funding information: National Key Research and Development Program of China (2023YFC2908304), and the Open Fund of State Key Laboratory of Vanadium and Titanium Resources Comprehensive Utilization (2021P4FZG02A).

Author contributions: All authors have accepted responsibility for the entire content of this manuscript and consented to its submission to the journal, reviewed all the results and approved the final version of the manuscript. JXW and ZYL designed the experiments and YZC and GW carried them out. HWY and GGJ are responsible for the testing and analysis of samples. SKN prepared the manuscript with contributions from all co-authors.

Conflict of interest: Authors state no conflict of interest.

References

[1] Taylor, P. R., S. A. Shuey, E. E. Vidal, and J. C. Gomez. Extractive metallurgy of vanadium-containing titaniferous magnetite ores: a

review. *Minerals & Metallurgical Processing*, Vol. 23, No. 8, 2006, pp. 80–86.
[2] Zhang, S. S., P. Hu, J. T. Rao, Z. Y. Wang, J. L. Zhang, and Y. B. Zong. Comprehensive utilization status of vanadium-titanium magnetite and feasibility analysis of Hismelt smelting. *Journal of Central South University*, Vol. 52, No. 9, 2021, pp. 3085–3092.
[3] Hao, Z. G., H. C. Fei, L. Lian, and T. Susan. Comprehensive utilization of vanadium-titanium magnetite deposits in china has come to a new level. *Acta Geologica Sinica*, Vol. 87, No. 1, 2012, pp. 286–287.
[4] Shuai, W., Y. F. Guo, T. Jiang, F. Chen, and F. Q. Zheng. Comprehensive utilization and industrial development direction of vanadium-titanium magnetite. *China Metallurgy*, Vol. 26, No. 10, 2016, pp. 40–44.
[5] Xu, L. J., L. Li, L. X. Chen, X. H. Li, and Z. L. Liu. Comprehensive recycling situation and development direction of vanadium-titanium magnetite in PanXi. *Sichuan Nonferrous Metals*, Vol. 1, 2011, pp. 1–5.
[6] Luo, J. H., H. Q. Ke, Y. C. Qiu, and P. C. Zhang. Studies of mineralogical characteristics on vanadium titanium magnetite in hongge area, Panzhihua, Sichuan, China. *Advanced Materials Research*, Vol. 813, 2013, pp. 292–297.
[7] Moskalyk, R. R. and A. M. Alfantazi. Processing of vanadium: a review. *Minerals Engineering*, Vol. 16, 2003, pp. 793–805.
[8] Safdar, F., Y. Zhang, S. L. Zheng, X. Chen, P. Sun, Y. Zhang, et al. Recovery of TiO_2-enriched material from vanadium titano-magnetite concentrates by partial carbon reduction and mild acid leaching. *Hydrometallurgy*, Vol. 193, 2020, id. 105324.
[9] Zhang, B. H., D. Y. Zou, K. H. Jin, and Q. C. Liu. Study of smelting reduction rate for vanadium titanium magnetite. *Acta Metallurgica Sinica*, Vol. 5, No. 4, 1992, pp. 229–234.
[10] Jiao, K. X., C. L. Chen, J. L. Zhang, Z. J. Liu, G. W. Wang, W. P. Wang, et al. Analysis of titanium distribution behaviour in vanadium-containing titanomagnetite smelting blast furnace. *Canadian Metallurgical Quarterly*, Vol. 2, 2018, pp. 1–9.
[11] Jiao, K. X., J. L. Zhang, Z. J. Liu, S. B. Kuang, and Y. X. Liu. Dissection investigation of Ti(C,N) behavior in blast furnace hearth during vanadium titano-magnetite smelting. *ISIJ International*, Vol. 57, No. 1, 2017, pp. 48–54.
[12] Yang, D., H. H. Zhou, J. Wang, Z. D. Pang, G. S. Pei, Z. M. Yan, et al. Influence of TiO_2 on viscosity, phase composition and structure of chromium-containing high titanium blast furnace slag. *Journal of Materials Research and Technology*, Vol. 12, 2021, pp. 1615–1622.
[13] Park, H., J. Y. Park, G. H. Kim, and I. Sohn. Effect of TiO_2 on the viscosity and slag structure in blast furnace type slags. *Steel Research International*, Vol. 83, No. 2, 2012, pp. 150–156.
[14] Huo, H. Y., G. Q. Liu, M. Zou, and G. Q. Ma. Discussion for comprehensive utilization of pangang high titanium blast furnace slag. *Rare Metal Materials and Engineering*, Vol. 39, 2010, pp. 134–137.
[15] Yang, D., H. H. Zhou, J. Wang, Z. D. Pang, G. S. Pei, Z. M. Yan, H. X. Mao, G. B. Qiu, and X. W. Lv. Influence of TiO2 on viscosity, phase composition and structure of chromium-containing high-titanium blast furnace slag. *Journal of Materials Research and Technology*, Vol. 8, 2021, pp. 1615–1622.
[16] Steinberg, W. S., W. Geyser, and J. Nell. The history and development of the pyrometallurgical processes at Evraz Highveld Steel & Vanadium. *Journal of the Southern African Institute of Mining and Metallurgy*, Vol. 111, No. 10, 2014, pp. 705–710.
[17] Qin, Q., G. G. Liu, Z. J. Li, J. L. Q. i Suryani, and E. A. Basuki. Comparison of several typical processes for dealing with vanadium titanium magnetite resources. *Mining and Metallurgy*, Vol. 23, No. 4, 2014, pp. 79–82.
[18] Shi, Q., J. Tang, and M. S. Chu. Optimal process parameters for direct carbothermal reduction of vanadium–titanium magnetite in a rotary kiln. *Steel Research International*, Vol. 94, No. 12, 2023, id. 2300176.
[19] Sadykhov, G. B. and I. A. Karyazin. Titanium–vanadium slags produced upon the direct reduction of iron from titanomagnetite concentrates. *Minerals & Metallurgical Processing*, Vol. 6, 2007, pp. 447–454.
[20] Shi, Y., D. Q. Zhu, J. Pan, Z. Q. Guo, S. H. Lu, and Y. X. Xue. Investigation into the coal-based direct reduction behaviors of various vanadium titanomagnetite pellets. *Journal of Materials Research and Technology*, Vol. 19, 2022, pp. 243–262.
[21] Zhang, B. H., Q. C. Liu, C. W. Li, D. Y. Zou, and J. B. Sun. Thermodynamics of v reduction in smelting reduction slag for vanadium-titanium containing magnetite. *Acta Metallurgica Sinica*, Vol. 29, No. 5, 1993, pp. 193–199.
[22] Roshchin, V. E., A. V. Asanov, and A. V. Roshchin. Possibilities of two-stage processing of titaniferous magnetite ore concentrates. *Russian Metallurgy*, Vol. 6, 2011, pp. 499–508.
[23] Chen, S. Y., J. Tang, M. S. Chu, P. H. Guo, and Y. T. Han. Pulverized reduction process of vanadium titanium magnetite . *Journal of Process Engineering*, Vol. 13, No. 2, 2013, pp. 60–64.
[24] Chen, S. Y. and M. S. Chu. A new process for the recovery of iron, vanadium and titanium from vanadium titano-magnetite. *Journal of the Southern African Institute of Mining and Metallurgy*, Vol. 116, No. 6, 2014, pp. 481–487.
[25] Wei, L., G. Q. Fu, M. S. Chu, and M. Y. Zhu. Reduction behavior and mechanism of Hongge vanadium titanomagnetite pellets by gas mixture of H_2 and CO. *Journal of Iron and Steel Research International*, Vol. 24, 2017, pp. 34–42.
[26] Hu, T., X. W. Lv, C. G. Bai, and G. B. Qiu. Isothermal reduction of titanomagnetite concentrates containing coal. *International Journal of Minerals, Metallurgy and Materials*, Vol. 21, No. 2, 2014, pp. 131–137.
[27] Hu, T., X. W. Lv, C. G. Bai, Z. G. Lun, and G. B. Qiu. Reduction behavior of panzhihua titanomagnetite concentrates with coal. *Metallurgical and Materials Transactions B: Process Metallurgy and Materials Processing Science*, Vol. 44, 2013, pp. 252–260.
[28] Zulhan, Z., Z. Husnaa, and E. A. Basuki. Effect of briquette thickness on iron nugget formation in fluxless processing of iron sand concentrate under isothermal-temperature gradient profiles. *ISIJ International*, Vol. 3, 2022, pp. 487–495.
[29] Zulhan, Z., C. L. Sutandar, I. Suryani, and E. A. Basuki. Effect of temperature patterns on iron nugget formation in fluxless processing of titanomagnetite. *Scientific reports-Uk*, Vol. 12, 2022, id. 8941.
[30] Chen, D. S., B. Song, L. N. Wang, T. Qi, and W. J. Wang. Direct reduction and enhanced reduction of vanadium-bearing titanomagnetite concentrates. *Journal of University of Science and Technology Beijing*, Vol. 33, No. 11, 2011, pp. 1331–1336.
[31] Chen, D. S., B. Song, L. N. Wang, T. Qi, and W. J. Wang. Solid state reduction of Panzhihua titanomagnetite concentrates with pulverized coal. *Minerals Engineering*, Vol. 24, 2011, pp. 864–869.
[32] Zhang, J. L., X. D. Xing, M. M. Cao, K. X. Jiao, C. L. Wang, and R. Shan. Reduction kinetics of vanadium titano-magnetite carbon composite pellets adding catalysts under high temperature. *Journal of Iron and Steel Research International*, Vol. 20, No. 2, 2013, pp. 1–7.
[33] Gao, E. X., Y. Z. Zhou, C. Geng, S. Y. Cui, T. C. Sun, and M. Jiang. Effects of CaF_2 on the direct reduction of beach titanomagnetite at different temperatures. *Environmental Progress & Sustainable Energy*, Vol. 42, No. 2, 2023, id. e14013.

[34] Jiang, T., J. Xu, S. F. Guan, and X. X. Xue. Study on coal-based direct reduction of high-chromium vanadium-titanium magnetite. *Journal of Northeastern University Natural Science*, Vol. 36, No. 1, 2015, pp. 77–80.
[35] Yang, J., T. Jiang, S. H. Ma, S. T. Yang, and M. Zhou. Kinetics and mechanism of coal-based direct reduction of high-chromium vanadium–titanium magnetite. *Journal of Iron and Steel Research International*, Vol. 29, No. 11, 2015, pp. 1723–1733.
[36] Chen, C., T. C. Sun, Y. Kou, and Y. Q. Zhao. Effect of magnesium on carbothermal reduction of vanadium-titanium magnetite concentrate. *Rare Metals*, Vol. 42, No. 7, 2018, pp. 765–771.
[37] Chen, C., T. C. Sun, X. P. Wang, and T. Y. Hu. Effects of MgO on the reduction of vanadium titanomagnetite concentrates with char. *JOM*, Vol. 69, No. 10, 2017, pp. 1759–1766.
[38] Li, R. M., L. Tao, Y. M. Zhang, J. Huang, and C. B. Xu. Efficient extraction of vanadium from vanadium–titanium magnetite concentrate by potassium salt roasting additives. *Minerals*, Vol. 8, 2018, id. 25.
[39] Li, R. M., L. Tao, Y. M. Zhang, and J. Huang. Mechanism of novel K_2SO_4/KCl Composite roasting additive for strengthening vanadium extraction from vanadium–titanium magnetite concentrate. *Minerals*, Vol. 8, 2018, id. 426.
[40] Li, J. Y., E. Tang, C. Qin, Q. Zhou, X. G. Fan, and J. Wang. Experimental research on deep reduction and grinding separation of low ti-bearing vanadium-titanium magnetite. *Iron Steel Vanadium Titanium*, Vol. 37, No. 5, 2016, pp. 25–29.
[41] Luo, Y. Partial phase diagram of Fe-Si (≤8wt-%)-C(≤0.1wt-%) and pseudobinary sections of Fe-Si and Fe-C. *Acta Metallurgica Sinica*, Vol. 24, No. 3, 1988, pp. 187–194.